*Pramana – J. Phys.* (2018) 90:49
https://doi.org/10.1007/s12043-018-1539-8



# Impact of depth and location of the wells on vibrational resonance in a triple-well system

ZHIJUAN CHEN and LIJUAN NING*

School of Mathematics and Information Science, Shaanxi Normal University, Xi'an 710119, China
*Corresponding author. E-mail: ninglijuan@snnu.edu.cn

MS received 3 September 2017; revised 1 November 2017; accepted 8 November 2017;
published online 7 March 2018

**Abstract.** The effect of depth and location of a triple-well potential on vibrational resonance is investigated in a quintic oscillator driven by a low-frequency force and a high-frequency force. The values of low-frequency $\omega$ and amplitude $g$ of the high-frequency force at which vibrational resonance occurs are derived both numerically and theoretically. It is found that: as $\omega$ varies, at most one resonance takes place and the response amplitude at resonance depends on the depth and the location of the potential wells. When $g$ is altered, the depth and location of wells can control the number of resonances, resulting in two, three and four resonances. The system parameters can be adjusted by controlling the depth and position of the wells to achieve optimum vibrational resonance. Furthermore, the changes induced by these two quantities in the tristable system are found to be richer than those induced in bistable systems.

**Keywords.** Vibrational resonance; triple-well potential; depth, location.

**PACS Nos** **46.40.Ff; 05.45.−a; 05.90.+ m; 05.45.Pq**

## 1. Introduction

The phenomenon of vibration resonance (VR) in nonlinear systems is of considerable interest in recent years. VR, which was originally introduced by Landa and McClintock [1], is commonly observed when a nonlinear system is subjected to two different external periodic signals and the response to a weak low-frequency signal can be maximised by modulating the high-frequency signal. It should be mentioned that nonlinear systems driven by biharmonic signals are ubiquitous in nature and cut across different fields, including neuroscience [2], laser physics [3], acoustics [4], brain dynamics [5] etc. Due to its potential applications, a large amount of research has been devoted to VR. Specifically, theoretical research to validate VR was implemented by Gitterman [6]. Experimental evidence of VR in a bistable vertical cavity laser system [7] and in an optical system [8] was provided by Chizhevsky *et al*. Through numerical simulation and experiment, it has been shown that VR is effective to enhance the detection and recovery of weak aperiodic binary signals in stochastic bistable systems [9]. Moreover, double VR was found in an asymmetric system [10,11] and single VR has been outlined in coupled oscillators [12] and complex network systems [13–15]. VR has also been reported in noise-induced structure [16] and FitzHugh–Nagumo model [17] . In addition to adjusting the amplitude of the high-frequency components of the external signal [18], the optimisation of resonance can also be achieved by controlling the fractional order [19,20] and the time delay [21,22].

Recently, interest in multiwell systems [23–27] is overwhelmingly increased because of its extensive applications, such as image sharpening [23], chemical kinetics [28], condensed matter physics [29], etc. The presence of VR in a damped quintic oscillator with triple-well potential was demonstrated by Jeyakumari *et al* [30]. Meanwhile, Yang and Liu proposed that such phenomenon also exists in a time-delayed multiwell system [31]. In ref. [32], Rajasekar *et al* extended VR to a system with periodic potential. Subsequently, VR was experimentally verified in a multistable vertical cavity surface-emitting laser system [33]. Besides, in engineering applications, as the complexity of the actual signal gradually emerges, it can be reasonably concluded that predicting and regulating the kinetic behaviour of nonlinear systems through the aid of system parameters has become an exigent problem. To the best of our knowledge, despite a number of papers devoted to theoretical

and numerical discussions of VR, the influence of the shape characteristics of the potential function had not been considered except in ref. [34], which emphasised some interesting features of VR in a symmetric double-well system wherein the depths and locations of minima of the wells were distinct. However, only a bistable system is described in this reference, and there is little work which studies this impact in other systems. Therefore, close attention should be paid to investigate the VR induced by the parameters of the potential function in a multistable system.

The main motivation of the present work is to precisely explore the effect of depth and location of the wells in a tristable system on the VR phenomenon, which is expected to provide the basis for further research of parameter-induced VR. In particular, given the flexibility of parameter adjustment and the ubiquity of multistable systems, this study may have practical applications in providing suitable regulation mechanisms of stationary states to achieve the desired VR effect in systems. The rest of the paper is structured as follows: §2 presents the model and provides a detailed theoretical analysis of VR in the model. In §3, theoretical expressions for control parameters at which VR takes place are obtained and the effect of the depth of the potential wells on VR is evaluated. Similarly, the influence of location of the potential wells on VR is discussed in §4. Finally, a brief conclusion is given in §5.

## 2. Model and theoretical predications

### 2.1 *Model*

The quintic oscillator model which has been introduced in detail in ref. [30] can be described as follows:

$$\ddot{x} + d\dot{x} + \frac{\mathrm{d}V(x)}{\mathrm{d}x} = f\cos(\omega t) + g\cos(\Omega t), \tag{1}$$

where

$$V(x) = \frac{1}{2}A\omega_0^2 x^2 + \frac{1}{4}B\beta x^4 + \frac{1}{6}C\gamma x^6. \tag{2}$$

Here, $d$ is the coefficient of linear damping; the terms $f\cos(\omega t)$ and $g\cos(\Omega t)$ stand for low-frequency input signal and a high-frequency signal with frequency $\Omega \gg \omega$, respectively. This model is encountered in various electrical and mechanical systems. In particular, the single- mode kinetics of a beam resting on an elastic substrate [35] can be described by eqs (1) and (2). It can also depict the single-mode kinetics of a beam under axial tension and resting on a nonlinear foundation.

For $\omega_0^2,\ \gamma,\ A,\ B,\ C > 0,\ \beta < 0$ with $\beta^2 > 4\omega_0^2\gamma$, the potential is of a symmetric triple-well form, as shown in figure 1. If the parameters $\omega_0^2 = 3, \beta = -4, \gamma = 1$ are fixed, system factors $A,\ B,\ C$ are considered. When $A = B = C = \alpha_1 > 0$, the potential has three minima at

$$x_1^* = 0, \quad x_{2,3}^* = \pm\sqrt{\frac{-\beta + \sqrt{\beta^2 - 4\gamma\omega_0^2}}{2\gamma}}$$

and two maxima at

$$x_{4,5}^* = \pm\sqrt{\frac{-\beta - \sqrt{\beta^2 - 4\gamma\omega_0^2}}{2\gamma}}.$$

The depth of the wells denoted by $\Delta V_l$ , $\Delta V_m$ and $\Delta V_r$ from left to right, respectively, are the same and equal to $\alpha_1(6\omega_0^2 p + 3\beta p^2 + 2\gamma p^3)/12$ where

$$p = \frac{-\beta - \sqrt{\beta^2 - 4\gamma\omega_0^2}}{2\gamma}.$$

The variation in the depth of the wells can be achieved by changing the parameter $\alpha_1$, where the values of $x_1^*$ and $x_{2,3}^*$ are kept constant, and this fact can be observed in figure 1a. On the other hand, for $A = 1/\alpha_2^2,\ B = 1/\alpha_2^4,\ C = 1/\alpha_2^6$ with $\alpha_2 \neq 0$, the minima of $V(x)$ are

$$x_1^* = 0, \quad x_{2,3}^* = \pm\alpha_2\sqrt{\frac{-\beta + \sqrt{\beta^2 - 4\gamma\omega_0^2}}{2\gamma}}$$

and the maxima are

$$x_{4,5}^* = \pm\alpha_2\sqrt{\frac{-\beta - \sqrt{\beta^2 - 4\gamma\omega_0^2}}{2\gamma}},$$

and in this case,

$$\Delta V_l = \Delta V_m = \Delta V_r = \frac{6\omega_0^2 p + 3\beta p^2 + 2\gamma p^3}{12}$$

is independent of $\alpha_2$. That is, the depth of the wells can remain unaltered while the distance between $x_1^*$ and $x_2^*$ (or $x_1^*$ and $x_3^*$) can be varied when $\alpha_2$ is changed, as displayed in figure 1b. In this work, attention has been paid to the impact of $\alpha_1$ and $\alpha_2$ on vibrational resonance, where $\alpha_1$ and $\alpha_2$ respectively indicate the properties of the depth and location of the potential wells. For convenience, system (1) with $A = B = C = \alpha_1$ and $A = 1/\alpha_2^2,\ B = 1/\alpha_2^4,\ C = 1/\alpha_2^6$ are represented by US1 and US2, respectively, and it is demanded that $\alpha_2$ be greater than zero.

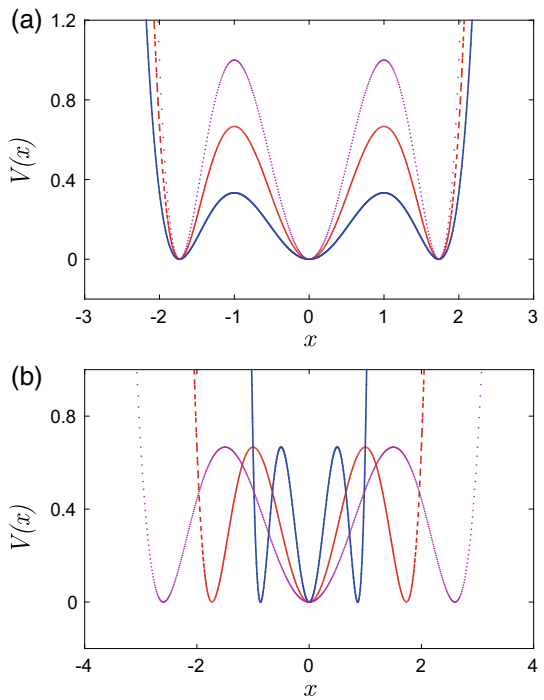


**Figure 1.** Triple-well potential of the quintic oscillator for (**a**) $A = B = C = \alpha_1$ and (**b**) $A = 1/\alpha_2^2, B = 1/\alpha_2^4, C = 1/\alpha_2^6$ with parameters $\omega_0^2 = 3, \beta = -4$ and $\gamma = 1$ fixed. In both the subplots, the values of $\alpha_1$ (**a**) and $\alpha_2$ (**b**) for continuous line, red dashed and pink dotted lines are 0.5, 1 and 1.5, respectively.

### 2.2 *Theoretical analysis for the response amplitude*

Under the assumption that $\Omega$ is much greater than $\omega$, the nonlinear system (1) can be processed via the method of direct separation of motion. Following this method [6], let

$$x(t) = X(t, \omega t) + \Psi(t, \Omega t), \tag{3}$$

where $X(t, \omega t)$ depicts the motion of the slow component. $\Psi(t, \Omega t)$ is a $2\pi$-periodic function of fast time $\tau = \Omega t$ and therefore has zero mean value as

$$\bar{\Psi}(t, \tau) = \frac{1}{2\pi}\int_0^{2\pi} \Psi(t, \tau)\mathrm{d}\tau = 0. \tag{4}$$

After substituting eq. (3) into eq. (1) and averaging over the fast time scale, the following equations of motion for $X$ and $\Psi$ can be obtained:

$$\begin{aligned}&\ddot{X} + d\dot{X} + (A\omega_0^2 + 3B\beta\overline{\Psi^2} + 5C\gamma\overline{\Psi^4})X \\ &\quad +10C\gamma\overline{\Psi^3}X^2 + (B\beta + 10C\gamma\overline{\Psi^2})X^3 \\ &\quad + C\gamma X^5 + B\beta\overline{\Psi^3} + C\gamma\overline{\Psi^5} \\ &= f\cos(\omega t),\end{aligned} \tag{5}$$

$$\begin{aligned}&\ddot{\Psi} + d\dot{\Psi} + A\omega_0\Psi + 3B\beta X^2(\Psi - \overline{\Psi}) \\ &\quad +3B\beta X(\Psi^2 - \overline{\Psi^2}) + B\beta(\Psi^3 - \overline{\Psi^3}) \\ &\quad +5C\gamma X^4(\Psi - \overline{\Psi}) + 10C\gamma X^3(\Psi^2 - \overline{\Psi^2}) \\ &\quad +10C\gamma X^2(\Psi^3 - \overline{\Psi^3}) + 5C\gamma X(\Psi^4 - \overline{\Psi^4}) \\ &\quad +C\gamma(\Psi^5 - \overline{\Psi^5}) \\ &= g\cos(\Omega t),\end{aligned} \tag{6}$$

where $\overline{\Psi^j} = (1/2\pi)\int_0^{2\pi} \Psi^j\,\mathrm{d}\tau,\ j = 0, 1, 2, ..., 5$. In the above two equations, our interest lies in eq. (5) for the slow variable, which can be adjusted properly through altering the parameters of the fast signal to prove the presence of VR. As $\Psi$ is a rapidly changing force, we further assume $\ddot{\Psi} \gg \dot{\Psi}, \Psi, \Psi^2, \Psi^3, \Psi^4, \Psi^5$. That is, eq. (6) can be approximated as $\ddot{\Psi} = g\cos(\Omega t)$ by utilising inertial approximation. $\Psi$ can be derived as follows:

$$\Psi = -\frac{g}{\Omega^2}\cos(\Omega t). \tag{7}$$

So $\overline{\Psi^2} = g^2/2\Omega^4, \overline{\Psi^3} = 0, \overline{\Psi^4} = 3g^4/8\Omega^8, \overline{\Psi^5} = 0$. Accordingly, eq. (5) turns to

$$\ddot{X} + d\dot{X} + c_1X + c_2X^3 + C\gamma X^5 = f\cos(\omega t), \tag{8}$$

where

$$\begin{aligned}c_1 &= A\omega_0^2 + \frac{3B\beta g^2}{2\Omega^4} + \frac{15C\gamma g^4}{8\Omega^8}, \\ c_2 &= B\beta + \frac{5C\gamma g^2}{\Omega^4}.\end{aligned} \tag{9}$$

The effective potential function of eq. (8) is

$$V_{\mathrm{eff}}(X) = \frac{1}{2}c_1X^2 + \frac{1}{4}c_2X^4 + \frac{1}{6}C\gamma X^6. \tag{10}$$

When there is no input signal, the equilibrium points of eq. (8) are given by

$$\begin{aligned}X_1^* &= 0,\ X_{2,3}^* = \pm\sqrt{\frac{-c_2 + \sqrt{c_2^2 - 4Cc_1\gamma}}{2C\gamma}}, \\ X_{4,5}^* &= \pm\sqrt{\frac{-c_2 - \sqrt{c_2^2 - 4Cc_1\gamma}}{2C\gamma}}.\end{aligned} \tag{11}$$

Slow oscillations may occur around these equilibrium states. Thus, the deviation $Y(t)$ of the slow motions $X(t)$ from the stable equilibrium point $X^*$ is introduced so that slow oscillations occur at about $Y^* = 0$. One has

$$\ddot{Y}+d\dot{Y}+\eta_1Y+\eta_2Y^2+\eta_3Y^3+\eta_4Y^4+C\gamma Y^5=f\cos(\omega t), \tag{12}$$

where

$$\eta_1 = c_1 + 3c_2X^{*2} + 5C\gamma X^{*4},$$
$$\eta_2 = 3c_2X^* + 10C\gamma X^{*3},$$
$$\eta_3 = c_2 + 10C\gamma X^{*2},$$
$$\eta_4 = 5C\gamma X^*. \tag{13}$$

Herein, as the low-frequency input signal satisfies the condition $f \ll 1$, we further consider that $|Y| \ll 1$ and neglect the nonlinear terms in eq. (12). Then, one can get $Y(t) = A_L \cos(\omega t - \phi)$, in which

$$A_L = \frac{f}{\sqrt{(\omega_r^2 - \omega^2)^2 + d^2\omega^2}},$$
$$\phi = \arctan\left(\frac{\omega^2 - \eta_1}{d\omega}\right) \tag{14}$$

and the resonant frequency $\omega_r = \sqrt{\eta_1}$. We can define the response amplitude of the system as

$$Q = \frac{A_L}{f} = \frac{1}{\sqrt{S}}, \tag{15}$$

where

$$S = \left(\omega_r^2 - \omega^2\right)^2 + d^2\omega^2. \tag{16}$$

Apparently, $Q$ is a quantitative indicator that signifies the extent of amplification of the weak input signal through the nonlinear system. On this basis, the resonance behaviour can be analysed. VR occurs when $Q$ reaches the local maximum, i.e., $S$ arrives at its local minimum.

## 3. Impact of depth of the potential wells on vibrational resonance

In this section, the role of depth of the potential wells on VR in system US1 is considered. According to the theoretical expression of $Q$, a local minimum of $S$ standing for a resonance is noted. By finding the minima of $S$, the value of $\omega_{\rm VR}$ or $g_{\rm VR}$ at which resonance occurs can be deduced.

First of all, we analyse the occurrence of resonance as $\omega$ is altered. Under the condition $S_\omega = {\rm d}S/{\rm d}\omega = (-4(\omega_r^2 - \omega^2) + 2d^2)\omega = 0$ and $S_{\omega\omega}|_{\omega=\omega_{\rm VR}} = {\rm d}^2S/{\rm d}\omega^2|_{\omega=\omega_{\rm VR}} > 0$, it is easily deduced that

$$\omega_{\rm VR} = \sqrt{\omega_r^2 - \frac{d^2}{2}}, \quad \omega_r^2 > \frac{d^2}{2}. \tag{17}$$

Once the values of other parameters are fixed and $\omega$ is increased from zero, the response amplitude $Q$ achieves its maximum at $\omega = \omega_{\rm VR}$. Resonance does not appear for $\omega_r^2 < d^2/2$. What is more interesting is that regardless of the extent to which $\omega$ changes, $\omega_r$ remains constant. So, a maximum of only one resonance can be observed.

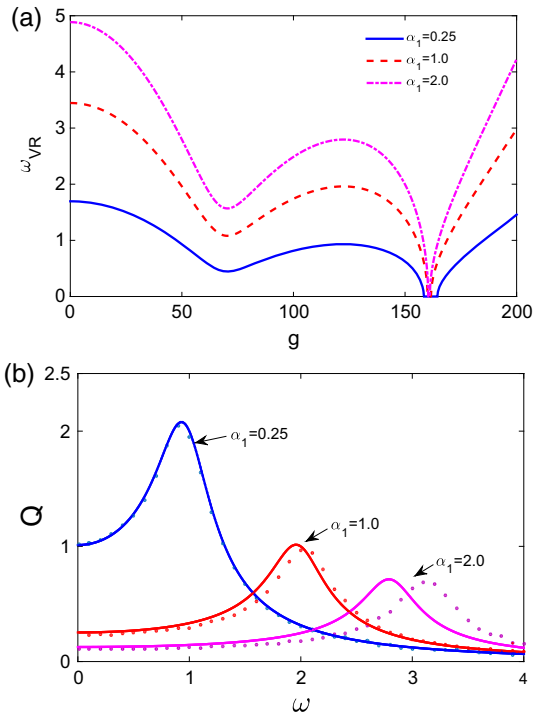


**Figure 2.** (**a**) Variation of $\omega_{\rm VR}$ vs. $g$ for different values of $\alpha_1$. (**b**) Response amplitude $Q$ as a function of $\omega$ for $g = 125$. Continuous lines are theoretical $Q$ while the coloured dots are numerically computed $Q$. The values of the other parameters are $\omega_0^2 = 3$, $\beta = -4$, $\gamma = 1$, $d = 0.5$, $f = 0.05$ and $\Omega = 10$.

In figure 2a, the influence of the depth of the potential wells on $\omega_{\rm VR}$ is discussed, where slow motions around $X_{2,3}^*$ are considered for the triple-well form of $V_{\rm eff}$. It is clear that $\omega_{\rm VR}$ becomes greater with the increase of $\alpha_1$ for a fixed value of $g$. Additionally, it can be seen that for $\alpha_1 = 0.25$, 1.0 and 2.0, the VR will not appear if $g \in [158.42, 164.56]$, $g \in [160.09, 161.61]$ and $g \in [160.36, 161.16]$, respectively (because $\omega_r^2 - d^2/2 < 0$ in the above regions of $g$). That is, the greater the depth is, the smaller the non-resonance interval of $g$ becomes, until it tends to zero.

Figure 2b demonstrates both theoretical and numerical response amplitude $Q$ as a function of $\omega$ for different values of $\alpha_1$. It presents only one peak on each curve, which means that only one resonance occurs. Furthermore, as the parameter $\alpha_1$ increases, the response amplitude $Q$ displays lower peaks and becomes more flat. This indicates that the depth of the well is too great, resulting in a less favourable output of the VR system. In order to verify the validity of theoretical predictions in figure 2b, numerical simulation results are calculated using the equation

$$Q = \frac{\sqrt{Q_s^2 + Q_c^2}}{f}, \tag{18}$$

with

$$Q_s = \frac{2}{nT}\int_0^{nT} x(t)\sin(\omega t)\mathrm{d}t,$$
$$Q_c = \frac{2}{nT}\int_0^{nT} x(t)\cos(\omega t)\mathrm{d}t, \tag{19}$$

where $T = 2\pi/\omega$ and $n$ is a positive integer. It can be plainly seen from figure 2b that the numerical results are in good agreement with the analytical ones. Next, the variable $g$ is treated as a controllable parameter. For US1 with $A = B = C = \alpha_1$, the bifurcation point that induces the changes in the number of stable steady states can be expressed as

$$g_0^{(1,2)} = \Omega^2\sqrt{\frac{-\beta \mp \sqrt{\beta^2 - (10\gamma\omega_0^2/3)}}{5\gamma/2}}. \tag{20}$$

The values $g = g_0^{(1)}$ and $g = g_0^{(2)}$ are independent of $\alpha_1$ and are critical points which make system (8) transit from tristability to bistability, and from bistability to monostability respectively. Then, we note that $g_{\mathrm{VR}}$ are the roots of the equation $S_g = \mathrm{d}S/\mathrm{d}g = 4(\omega_r^2 - \omega^2)\omega_r\omega_{rg} = 0$ with $S_{gg}|_{g=g_{\mathrm{VR}}} = \mathrm{d}^2S/\mathrm{d}g^2|_{g=g_{\mathrm{VR}}} > 0$, where $\omega_{rg} = \mathrm{d}\omega_r/\mathrm{d}g$. For $g > g_0^{(2)}$, $V_{\mathrm{eff}}$ remains a single-well potential, and slow oscillation occurs around $X_1^* = 0$. Under the circumstances, one obtains $g_{\mathrm{VR}}^{(1)}$ from $\omega_r^2 - \omega^2 = 0$

$$g_{\mathrm{VR}}^{(1)} = \Omega^2\sqrt{\frac{-\alpha_1\beta + \sqrt{\alpha_1^2\beta^2 - 10\alpha_1\gamma(\alpha_1\omega_0^2 - \omega^2)/3}}{5\alpha_1\gamma/2}},$$
$$\alpha_1 > 0. \tag{21}$$

For $g_0^{(1)} \le g \le g_0^{(2)}$, $V_{\mathrm{eff}}$ turns to a double-well potential and slow oscillations appear around $X_{2,3}^*$, and for $g < g_0^{(1)}$, $V_{\mathrm{eff}}$ is a triple-well potential and slow motions take place around $X_{1,2,3}^*$. In the above two cases, VR can be observed when either $\omega_r^2 - \omega^2 = 0$ or $\omega_{rg} = 0$ with $S_{gg} > 0$. As $\omega_r$ is a complicated function of $g$, it is difficult to derive the theoretical expression of $g$ at which VR takes place. Consequently, $g_{\mathrm{VR}}^{(2)}$ and $g_{\mathrm{VR}}^{(3)}$, which correspond to double-well and triple-well cases of the $V_{\mathrm{eff}}$ respectively, can be ascertained numerically from eq. (16).

In addition, it is worth pointing out that resonance in the double-well Duffing oscillator (i.e., $\gamma = 0$ in eq. (1)) can only occur when $\omega_r^2 - \omega^2 = 0$ with $S_{gg} > 0$, which is shown in ref. [34]. However, for the triple-well systems considered in this work, resonance can be observed not only when $\omega_r^2 - \omega^2 = 0$ but also when $\omega_{rg} = 0$ with $S_{gg} > 0$. Thus, the related issues will be discussed here.

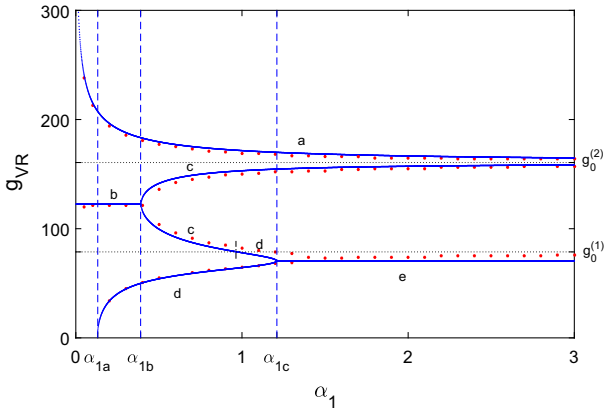


**Figure 3.** $g_{\mathrm{VR}}$ as a function of $\alpha_1$ in US1. Continuous lines are theoretical $g_{\mathrm{VR}}$ while the red dots are numerically computed $g_{\mathrm{VR}}$ from eq. (18).

In figure 3a, the impact of the depth of the wells on $g_{\mathrm{VR}}$ is investigated. Curves a–e are obtained from the following cases:

(1) Curve a: $g > g_0^{(2)}$ and $\omega_r^2 - \omega^2 = 0$,
(2) Curve b: $g_0^{(1)} \le g \le g_0^{(2)}$ and $\omega_{rg} = 0$,
(3) Curve c: $g_0^{(1)} \le g \le g_0^{(2)}$ and $\omega_r^2 - \omega^2 = 0$,
(4) Curve d: $0 < g < g_0^{(1)}$ and $\omega_r^2 - \omega^2 = 0$,
(5) Curve e: $0 < g < g_0^{(1)}$ and $\omega_{rg} = 0$,

where $g_{\mathrm{VR}}^{(1)}$, $g_{\mathrm{VR}}^{(2)}$ and $g_{\mathrm{VR}}^{(3)}$ are represented by curve a, both curves b and c, and curves d and e, respectively. In this figure, it is of interest that the number of resonance and values of $g_{\mathrm{VR}}$ is dominated by the parameter $\alpha_1$. More specifically, two resonance curves $g_{\mathrm{VR}}^{(1)}$ and $g_{\mathrm{VR}}^{(2)}$ can be observed when $0 < \alpha_1 < \alpha_{1a} = 0.132$. $g_{\mathrm{VR}}^{(3)}$ begins to appear as $\alpha_1$ increases from $\alpha_{1a}$ to $\alpha_{1b}$. For $\alpha_{1b} = 0.39 < \alpha_1 < \alpha_{1c} = 1.21$, the resonance curves change from three to four; this is mainly because $g_{\mathrm{VR}}^{(2)}$ or $g_{\mathrm{VR}}^{(3)}$ may have two values. When $\alpha_1$ exceeds a certain threshold value ($\alpha_{1c}$), the curve again becomes three.

In order to reach a better understanding of the various curves in figure 3, $\omega_r$ and $\omega_{rg}$ as functions of $g$ are presented in figure 4. Concrete analysis is as follows: First, for each fixed value of $\alpha_1$, the plot of $\omega_r$ in figure 4a has a local minimum at $g = g_1 = 70.4$ and a local maximum at $g = g_2 = 122.4$. Meanwhile, $\omega_{rg}$ is equal to zero at these two extrema, as stated in figure 4b. Secondly, when $\alpha_1 = 0.12 < \alpha_{1a}$, an interesting finding in figure 4a is that the horizontally dashed $\omega = 1.25$ intersects the resonance curve $\omega_r$ only at $g = 210.2$. $Q$ arrives at a local maximum at this value of $g$ with $\omega_r^2 - \omega^2 = 0$ and $Q_{\max} = 1/(\mathrm{d}\omega) = 1.6$. Also note that $\omega_r$ reaches a local minimum at $g = g_1 < g_0^{(1)}$, where resonance occurs owing to $\omega_{rg} = 0$. The value of $Q$

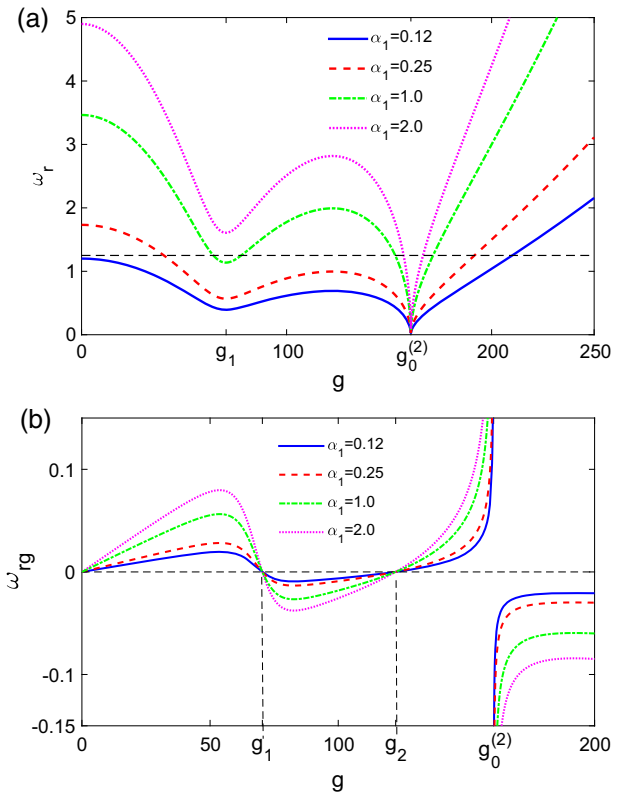


**Figure 4.** Plot of (**a**) $\omega_r$ and (**b**) $\omega_{rg}$ as a function of the control parameter $g$. The horizontal dashed line stands for $\omega_r = \omega = 1.25$ in (**a**).

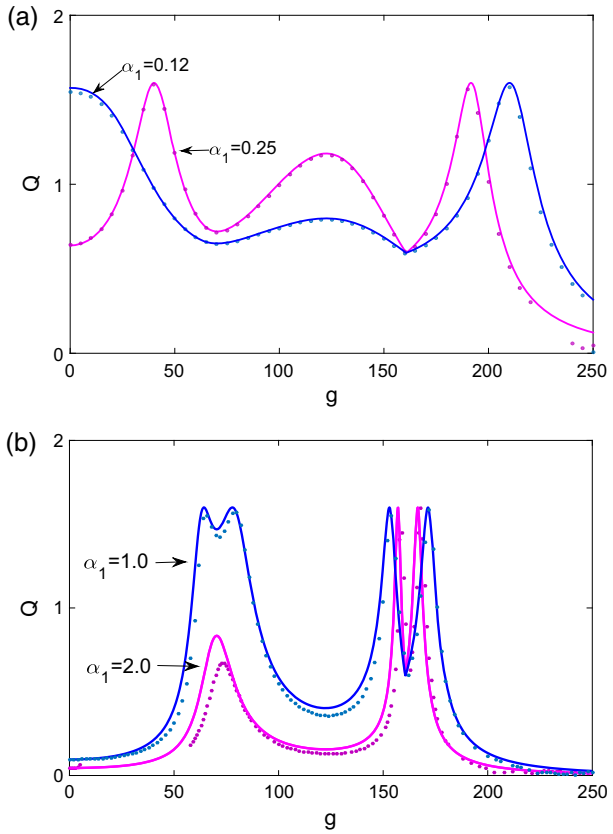


**Figure 5.** (**a**) and (**b**) Plot of $Q$ vs. $g$ for four values of $\alpha_1$ with $d = 0.5$. Continuous lines represent theoretical results obtained from eq. (15). Coloured dots illustrate the numerically calculated $Q$ from eq. (18).

at this resonance is lower than its value at $g = 210.2$. The trend of $Q$ is shown in figure 5. Double resonance at $g = g_1$ and 210.2 for $\alpha_1 = 0.12$ was displayed in figure 5a. Thirdly, When $\alpha_{1a} < \alpha_1 = 0.25 < \alpha_{1b}$, triple resonance occurs. In conjunction with figure 3, it can be discovered that there is a resonance at $g = g_2$ even though $\omega_r \neq \omega$. Beyond that, two more resonances appear, one at $g = 40.2$ and the other at $g = 191.8$, due to the fact that resonant frequency $\omega_r$ matches with frequency $\omega$ of the input signal. An instance of triple resonance is shown in figure 5a for $\alpha_1 = 0.25$. And for $\alpha_1 = 2.0$, a similar discussion can be made. Finally, when $\alpha_{1b} < \alpha_1 = 1.0 < \alpha_{1c}$, the curve $\omega_r$ intersects the dashed line $\omega = 1.25$ at four values of $g$. In other words, if the condition $\omega_r^2 - \omega^2 = 0$ is satisfied, quadruple resonance is noticed. In addition, when $Q_{\max} = 1/(\mathrm{d}\omega) = 1.6$, four resonances, all with the same $Q$ for $\alpha_1 = 1.0$, are shown in figure 5b.

## 4. Impact of location of the potential wells on vibrational resonance

Analogously, the effect of location of the wells on VR in system US2 can be explored. For US2 with $A = 1/\alpha_2^2$, $B = 1/\alpha_2^4$ and $C = 1/\alpha_2^6$, with the increase of $\alpha_2$, the position of the two maxima of $V(x)$ gradually shift away from the origin in the reverse direction and the distance between the neighbouring potential wells also increases. In view of such a situation, one can obtain

$$g_0^{(1,2)} = \alpha_2 \Omega^2 \sqrt{\frac{-\beta \mp \sqrt{\beta^2 - (10\gamma\omega_0^2/3)}}{5\gamma/2}}, \tag{22}$$

$$g_{\mathrm{VR}}^{(1)} = \Omega^2 \left( \alpha_2 \sqrt{\frac{-2\beta}{5\gamma}} + \sqrt{\frac{\sqrt{\alpha_2^{-2}\beta^2 - 10\gamma(\alpha_2^{-2}\omega_0^2 - \omega^2)/3}}{5\alpha_2^{-3}\gamma/2}} \right), \quad \alpha_2 \neq 0. \tag{23}$$

$g_{\mathrm{VR}}^{(2)}$ and $g_{\mathrm{VR}}^{(3)}$ are given by the numerical calculation of eq. (16). Obviously, based on eq. (22), the bifurcation points $g_0^{(1,2)}$ depend on $\alpha_2$. Also, $\omega_{\mathrm{VR}}$ can be obtained from eq. (17).

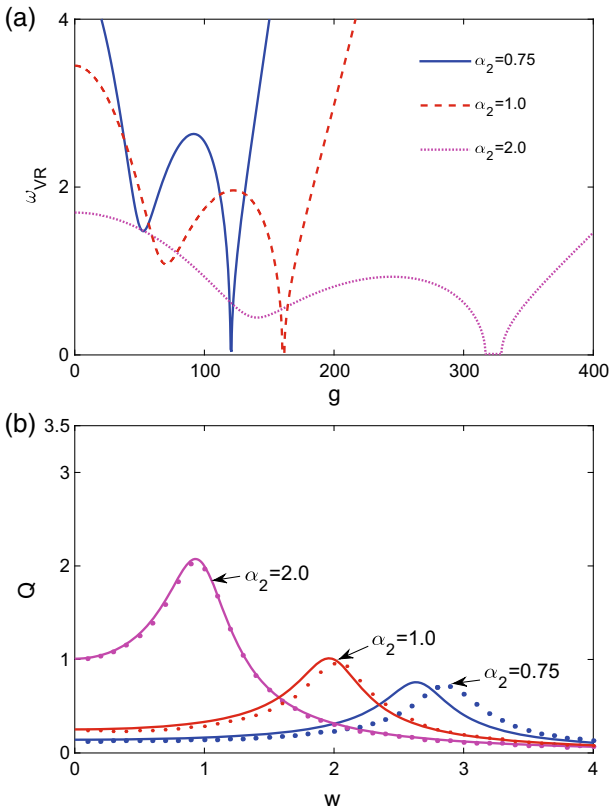


**Figure 6.** (**a**) Variation of $\omega_{\mathrm{VR}}$ vs. $g$ for different values of $\alpha_2$. (**b**) Plot of $Q$ vs. $\omega$ for a fixed value of $g$. The values of $g$ for $\alpha_2 = 0.75,\ 1.0$ and 2.0 are 91.76, 122.08 and 244.71 respectively. Continuous lines are theoretical $Q$ and the coloured dots are numerically computed $Q$. The simulation parameters are $\omega_0^2 = 3, \beta = -4, \gamma = 1, d = 0.5$ and $\Omega = 10$.

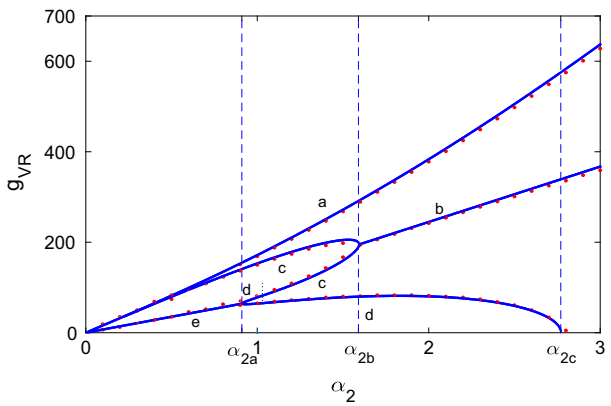


**Figure 7.** $g_{\mathrm{VR}}$ as a function of $\alpha_2$ in US2. Continuous lines are theoretical $g_{\mathrm{VR}}$ and the coloured dots are numerical $g_{\mathrm{VR}}$. Curve a, curves b and c, and curves d and e denote $g_{\mathrm{VR}}^{(1)}$, $g_{\mathrm{VR}}^{(2)}$ and $g_{\mathrm{VR}}^{(3)}$, respectively.

In figure 6a, $\omega_{\mathrm{VR}}$ is plotted as a function of $g$ for different values of $\alpha_2$. It is revealed that VR is not observed within a certain range of $g$. Moreover, it

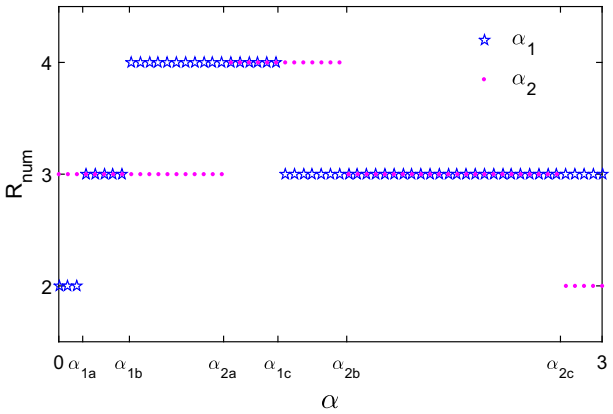


**Figure 8.** Variation of the number of resonance peaks $R_{\mathrm{num}}$ vs. $\alpha_1$ and $\alpha_2$ for various values of $g$.

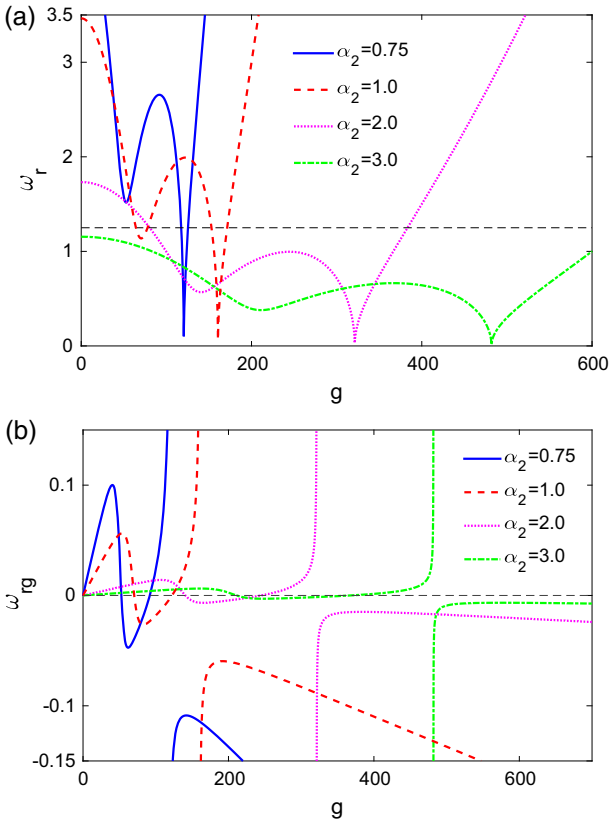


**Figure 9.** Plot of (**a**) $\omega_r$ and (**b**) $\omega_{rg}$ as a function of $g$ for different values of $\alpha_2$. The horizontal dashed line stands for $\omega_r = \omega = 1.25$ in (**a**).

can be seen from figure 6a that the increase of $\alpha_2$ can lead to greater non-resonance intervals of $g$ and a change in the positions of these intervals. By making a comparison between US1 and US2, we can conclude that the location parameter $\alpha_2$ affects not only the length of the non-resonance interval but also the position of the interval, and the depth parameter $\alpha_1$

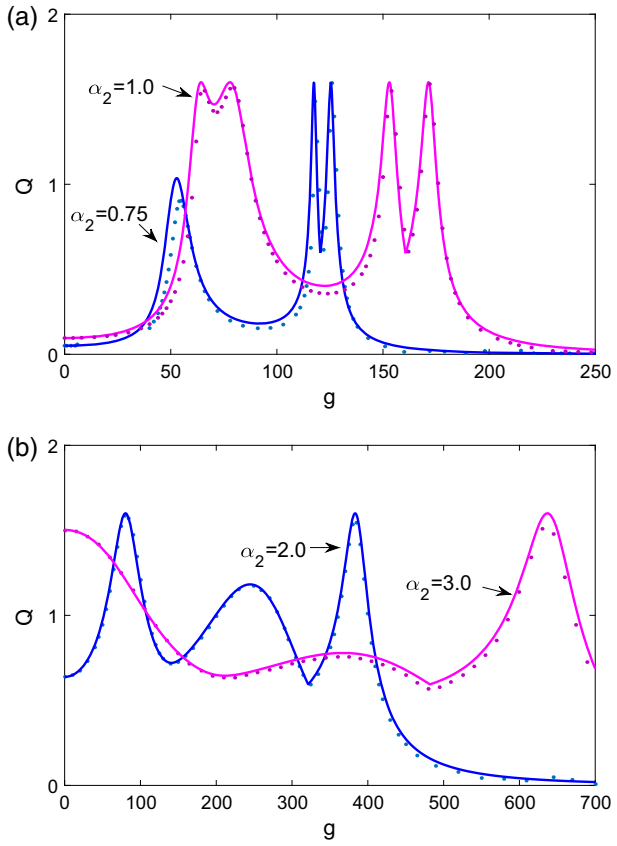


**Figure 10.** (**a**) and (**b**) Plot of $Q$ vs. $g$ for four values of $\alpha_2$ with $d = 0.5$. Continuous lines represent theoretical results. Coloured dots represent numerically calculated $Q$.

only impacts the former. Figure 6b presents the evolution of response amplitude $Q$ vs. low-frequency $\omega$, which manifests in the response $Q$ peak becoming higher and the position of the peak gradually moving to the origin as $\alpha_2$ increases from 0.75 to 2.0. This shows that when the distance between the neighbouring wells is larger, the particles can complete the jump better and initiate a satisfactory output response in the VR system. Conversely, with the increase of the depth parameter, the peak of $Q$ in US1 decreases and the position of the peak becomes farther from the origin.

Figure 7 provides analytical and numerical results of $g_{\rm VR}$ for a range of $\alpha_2$. For $0 < \alpha_2 < \alpha_{2a}$, triple resonance occurs, while for $\alpha_{2a} < \alpha_2 < \alpha_{2b}$, there is a quadruple resonance, and it again becomes triple resonance for $\alpha_{2b} < \alpha_2 < \alpha_{2c}$. For the three kinds of cases, $g_{\rm VR}^{(1)}$, $g_{\rm VR}^{(2)}$ and $g_{\rm VR}^{(3)}$ always exist, although the number of values of $g_{\rm VR}^{(2)}$ and $g_{\rm VR}^{(3)}$ are altered. As $\alpha_2$ further increases, one has both $g_{\rm VR}^{(1)}$ and $g_{\rm VR}^{(2)}$ at the same time, which means that double resonance appears. In addition, comparing figure 3 with figure 7, we find that the number of resonances varies in the opposite way. As $\alpha_1$ and $\alpha_2$ increase, in US1, three resonances appear initially, followed by four and three resonances, then finally two resonances. On the other hand, in US2, the resonance changes from triple to quadruple, then again to triple, then finally becomes double. These results can also be observed in figure 8, where we plot the variation of the number of resonance peaks with the depth parameter $\alpha_1$ and the location parameter $\alpha_2$.

The variation of $\omega_r$ and $\omega_{rg}$ with $g$ for four values of $\alpha_2$ are demonstrated in figure 9. In figure 9, one can easily see that the critical points $g_0^{(1,2)}$ always change with $\alpha_2$, which is different from the bifurcation points in US1 that are independent of the depth parameter $\alpha_1$. The response of $Q$ to four fixed values of $\alpha_2$ is displayed in figure 10 corresponding to other given parameters, which depicts the number of resonances with the increase in $g$. It is evident that there are three resonances for $\alpha_2 = 0.75$ and $\alpha_2 = 2.0$, two resonances for $\alpha_2 = 3.0$, and four resonances for $\alpha_2 = 1.0$.

## 5. Conclusion

To conclude, the effect of depth of the wells and the distance between the neighbouring wells is systematically studied in a quintic oscillator which has triple-well potential. Unlike a bistable system [34], resonance is also discovered at $\omega_{rg} = 0$ in a tristable system. This means that depth and position of the wells have a richer impact on the systems studied in this paper. From the theoretical expression of $Q$, we are able to determine the values of $\omega$ and $g$ at which VR occurs. If $\omega$ is a controllable parameter, we found either no resonance or one resonance according to the values of other parameters of US1 and US2, and that the response amplitude $Q = Q_{\rm max}$ at resonance is dependent on the quantities of $\alpha_1$ and $\alpha_2$. Nevertheless, if $g$ is treated as a variable, multiple resonance is noticed in systems US1 and US2. Both $\alpha_1$ and $\alpha_2$ can induce these changes in the value of $g_{\rm VR}$ and in the number of resonances. Thus, we can observe that changing the depth and location of wells can affect the characteristics of VR. In other words, the system parameters can be adjusted by controlling the above two quantities to achieve an optimum VR state.

The response amplitude of the output is closely related to the potential well in which the motion takes place. Therefore, it is meaningful to analyse the different effects of the depth and position of the wells on the VR. Based on the above analysis, we trust that the proposed

regulation strategies can possibly be preferred in some domains such as nonlinear optics.

## Acknowledgements

This work was supported by the National Natural Science Foundation of China (Grant No. 11202120) and the Fundamental Research Funds for the Central Universities (Grant Nos GK201502007 and GK201701001).

## References

[1] P S Landa and P V E McClintock, *J. Phys. A: Math. Gen*. **33**, L433 (2000)
[2] J D Victor and M M Conte, *Visual Neurosci*. **17**, 959 (2000)
[3] D C Su, M H Chiu and C D Chen, *Precis. Eng*. **18**, 161 (1993)
[4] A O Maksimov, *Ultrasonics* **35**, 79 (1997)
[5] A Knoblauch and G Palm, *Biosystems* **79**, 83 (2005)
[6] M Gitterman, *J. Phys. A: Math. Gen*. **34**, L355 (2001)
[7] V N Chizhevsky and G Giacomelli, *Phys. Rev. A* **71**, 011801 (2005)
[8] V N Chizhevsky, E Smeu and G Giacomelli, *Phys. Rev. Lett*. **91**, 220602 (2003)
[9] V N Chizhevsky and G Giacomelli, *Phys. Rev. E* **77**, 051126 (2008)
[10] S Jeyakumari, V Chinnathambi, S Rajasekar and M A F Sanjuan, *Int. J. Bifurc. Chaos* **21**, 275 (2011)
[11] T O Roylayinde, J A Laoye, O O Popoola and U E Vincent, *Chaos* **26**, 093117 (2016)
[12] V Gandhimathi, S Rajasekar and J Kurths, *Phys. Lett. A* **360**, 279 (2006)
[13] B Deng, J Wang and X Wei, *Chaos* **19**, 013117 (2009)
[14] B Deng, J Wang, X Wei, K M Tsang and W L Chan, *Chaos* **20**, 013113 (2010)
[15] J Shi, C Huang, T Dong and X Zhang, *Phys. Biol*. **7**, 036006 (2010)
[16] A A Zaikin, L Lopez, J P Baltanas, J Kurths and M A F Sanjuan, *Phys. Rev. E* **66**, 011106 (2002)
[17] E Ullner, A Zaikin, J Garcia-Ojalvo, R Bascones and J Kurths, *Phys. Lett. A* **312**, 348 (2003)
[18] I I Blekhman and P S Landa, *Int. J. Non-linear Mech*. **39**, 421 (2004)
[19] J H Yang and H Zhu, *Chaos* **22**, 013112 (2012)
[20] J H Yang, M A F Sanjuan, W Xiang and H Zhu, *Pramana – J. Phys.* **81**, 943 (2013)
[21] C Jeevarathinam, S Rajasekar and M A F Sanjuan, *Chaos* **23**, 013136 (2013)
[22] D Hu, J Yang and X Liu, *Commun. Nonlinear Sci.* **17**, 1031 (2012)
[23] G Gilboa, N Sochen and Y Y Zeevi, *J. Math. Imaging Vision* **20**, 121 (2004)
[24] C Wagner and T Kiefhaber, *Proc. Natl Acad. Sci. USA* **96**, 6716 (1999)
[25] S Arathi and S Rajasekar, *Phys. Scr.* **84**, 065011 (2011)
[26] P K Ghosh, B C Bag and D S Ray, *Phys. Rev. E* **75**, 032101 (2007)
[27] S Rajasekar and M A F Sanjuan, *Nonlinear resonances* (Springer, 2016)
[28] P K Ghosh, B C Bang and D S Ray, *J. Chem. Phys.* **127**, 044510 (2004)
[29] F Bouthanoute, L El Arroum, Y Boughaleb and M Mazroui, *Moroccan J. Condens. Matter* **9**, 17 (2007)
[30] S Jeyakumari, V Chinnathambi, S Rajasekar and M A F Sanjuan, *Chaos* **19**, 043128 (2009)
[31] J H Yang and X B Liu, *Chaos* **20**, 033124 (2010)
[32] S Rajasekar, K Abirami and M A F Sanjuan, *Chaos* **21**, 033106 (2011)
[33] V N Chizhevsky, *Phys. Rev. E* **89**, 062914 (2014)
[34] S Rajasekar, S Jeyakumari, V Chinnathambi and M A F Sanjuan, *J. Phys. A: Math. Theor.* **43**, 465101 (2010)
[35] S Lenci, G Menditto and A M Tarantino, *Int. J. Non-Linear Mech.* **34**, 615 (1999)